CARBON 81 (2015) 497–504

Available at www.sciencedirect.com

ScienceDirect

journal homepage: www.elsevier.com/locate/carbon

High strength measurement of monolayer graphene oxide

Changhong Cao [a,1], Matthew Daly [b,1], Chandra Veer Singh [b,*], Yu Sun [a,*], Tobin Filleter [a,*]

[a] Department of Mechanical and Industrial Engineering, University of Toronto, Toronto, ON M5S 3G8, Canada
[b] Department of Materials Science and Engineering, University of Toronto, Toronto, ON M5S 3E4, Canada

ARTICLE INFO

Article history:
Received 16 August 2014
Accepted 28 September 2014
Available online 5 October 2014

ABSTRACT

In this study, the strength of monolayer graphene oxide membranes was experimentally characterized. The monolayer GO membranes were found to have a high carbon-to-oxygen ratio (~4:1) and an average strength of 17.3 N/m (24.7 GPa). This measured strength is orders of magnitude higher than previously reported values for graphene oxide paper and is approximately 50% of the 2D intrinsic strength of pristine graphene. In order to corroborate strength measurements, experimental values were compared to theoretical first-principles calculations. Using a supercell constructed from experimental measurements of monolayer graphene oxide chemistry and functional structure, density functional theory calculations predicted a theoretical strength of 21.9 N/m (31.3 GPa) under equibiaxial tension, in good agreement with the experimental data. Furthermore, computational simulations were used to understand the underlying fracture mechanism, in which bond cleavage occurred along a path connecting oxygenated carbon atoms in the basal plane. This work shows that monolayer graphene oxide possesses near-theoretical strength reaching tens of GPa.

1. Introduction

Graphene oxide (GO) can be produced at a low cost (as compared to graphene) from bulk graphite using well-known methods developed by Brodie [1], Staudenmeier [2] and Hummer [3], and has excellent dispersibility in many solvents, permitting the synthesis of low-cost solution chemistries [2–4] and easy deposition on various substrates [5]. Furthermore, the functional groups of GO may be chemically, thermally or electrochemically engineered, leading to tunable physicochemical properties [6]. So far, GO has shown great promise as a candidate for various engineering applications [6,7]. In order to further encourage implementation of GO in engineering applications, a rigorous characterization of its mechanical properties is of critical importance. Graphene, for example, has been the subject of significant research interest with experimental studies reporting its intrinsic strength to be above 100 GPa [8,9]. Additionally, an experimental study of defective graphene has shown that mechanical properties are not drastically sensitive to the changes in bond hybridization resulting from oxygenation [10]. Furthermore, computational studies have added a rich understanding of the effects of vacancies [11,12] and bond reconstructions [13,14] on the mechanical properties of graphene.

* *Corresponding authors.*
E-mail addresses: chandraveer.singh@utoronto.ca (C.V. Singh), sun@mie.utoronto.ca (Y. Sun), filleter@mie.utoronto.ca (T. Filleter).
[1] These authors contributed equally to this work.
http://dx.doi.org/10.1016/j.carbon.2014.09.082
0008-6223/

In comparison to graphene, however, experimental investigations of the mechanical properties of monolayer GO are limited, despite widespread implementation of GO films as a stiffening and strengthening additive in composite applications [15,16]. The 3D elastic modulus of monolayer GO membranes has been experimentally characterized and is reported to be approximately ~25% of pristine graphene [17,18]; however, the strength of monolayer GO has not been experimentally measured to date [19]. Computational studies have predicted that the strength of monolayer GO could be as high as approximately 50% of the intrinsic strength of pristine graphene [20,21]. Currently, only the strength of GO paper (micrometers thick) has been experimentally studied [22,23]. Relative to other macroscopic materials, the comparatively large strengths measured for GO papers and GO reinforced composites are often attributed to the high predicted strength of monolayer GO. However, their strengths are still far below the theoretically estimates; with fracture stresses in the MPa range typically reported [22–24].

In this study, we evaluate the strength of monolayer GO through atomic force microscopy (AFM) nanoindentation combined with a continuum modeling approach. Specifically, analytical fitting as well as continuum-based simulations are used to analyze experimental AFM nanoindentation load–displacement data, permitting direct strength assessment from comparison to AFM breaking load measurements. Independent density functional theory (DFT) calculations are also performed to corroborate strength measurements as well as identify fracture mechanisms in the monolayer GO membranes.

2. Experimental and computational methodology

2.1. Graphene oxide sample preparation

Graphene Oxide flakes (Cheaptube Inc.) synthesized by a modified Hummer's method [3] were used as the precursor material. 1 mg of the GO flake mixed with 10 mL of deionized water was slowly stirred for one week using a magnetic stirrer. The upper portion of the solution was diluted and centrifuged at 3000 rpm for 10 min. The aqueous solution was further centrifuged at 5000 rpm for 10 min. The solution, obtained by mixing the precipitate with de-ionized water, was used for drop-casting onto a silicon nitride transmission electron microscopy (TEM) grid which had an array of through-holes (2.5 μm in diameter and 2 μm spacing). Dried in air, the GO flake was observed to be well-positioned over the grid, covering a number of holes and yielding several suspended GO membranes for testing (see Supplementary data, Fig. S1).

2.2. Atomic force microscopy nanoindentation protocol

AFM nanoindentation studies were performed using an Asylum Research MFP-3D instrument. The radius of the monolithic diamond AFM probe (Nanoscience Inc., ND-DYI Series) was measured by scanning electron microscopy to be ~102 nm (see Supplementary data, Fig. S2). The spring constant of the cantilever was calibrated and measured to be 34.24 N/m (see Section S1 of the Supplementary data). All nanoindentation experiments were conducted at ~24 °C with a ~30% relative humidity. In order to collect topological images, non-intrusive tapping mode scanning was utilized. After image collection, the probe was retracted from the sample and the instrument was switched into contact mode for nanoindentation. Elastic measurements were performed through load-controlled indentation to 100 nN and then subsequent unloading. Tapping mode scanning was then performed to confirm the integrity of the membranes, which were all found to be undamaged after elastic loading. Subsequently, GO membranes were indented until fracture, after which a post-mortem image of the failed membrane was collected using tapping mode. All loading measurements were collected from nanoindentation tests performed on a relatively large GO flake suspended over several holes in the TEM grid (see Supplementary data, Fig. S1). The same AFM probe was used for each measurement.

2.3. Finite element analysis

The ABAQUS software package was used to perform Finite Element Method (FEM) nanoindentation simulations. Monolayer GO membranes, with a 2.5 μm diameter and an assumed thickness of 0.7 nm (see Section 3.1), were constructed for FE analysis. The AFM probe was modeled as a rigid hemisphere with a radius of 102 nm (see Supplementary data, Fig. S2) and the contact between the indenter tip and GO membrane was assumed to be frictionless. Consistent with previous studies, the GO membrane was assumed to be isotropic with a Poisson's ratio of 0.165 [18], which is the value for graphite. The elastic modulus obtained from fitting of experimental data was used to model membrane stiffening (see Section 3.1). The equibiaxial prestress obtained from analytical fitting was applied in the membrane plane prior to nanoindentation. An 8 node linear brick element was used for meshing of the GO membranes. A mesh sensitivity analysis was performed to ensure convergence of simulation results. Stress is reported as the maximum in-plane component of the Cauchy tensor.

2.4. Density functional theory calculations

Quantum mechanical simulations were performed using the freely available Quantum Espresso software suite [25] with a Perdew–Burke–Ernzerhof generalized gradient approximation (PBE-GGA) exchange–correlation functional [26] and ultrasoft pseudopotentials. A plane-wave basis set with a kinetic energy cutoff of 45 Ry (612.26 eV) and an $8\times8\times1$ Monkhorst–Pack k-point grid were utilized. The simulation supercell possessed 38 atoms. Prior to loading, system energy was minimized using variable cell relaxation under a conjugate gradient algorithm with a convergence criterion of 0.0001 Ry/Bohr (0.0051 eV/Å). A supercell height of 45 Å was maintained orthogonal to the basal plane of the GO membrane to avoid electronic interactions between periodic images of the DFT supercell. The fully relaxed DFT supercell was then dilated in 1% increments to different levels of engineering strain. After application of each strain increment, the deformed structure was relaxed to a minimum energy configuration, while holding supercell dimensions fixed.

Stresses were computed in terms of force per unit area at the cross-sectional edges of the simulation cell, and represent the true or Cauchy stresses. A 0.7 nm membrane thickness (see Section 3.1) was assumed for all 3D stress calculations of monolayer GO in DFT simulations.

3. Results and discussion

3.1. *Structural characterization & atomic force microscopy nanoindentation studies*

A representative bright field TEM (JEOL 2010) image revealed that the suspended membrane structures were flat and clean, without wrinkles or indication of voids (Fig. 1a). Selected area electron diffraction (SAED) patterns were obtained for each sample to confirm that the tested GO membranes were single layers as demonstrated by the presence of only six sharp diffraction spots, corresponding to the monolayer GO honeycomb lattice (Fig. 1b) [18]. Raman spectra (Renishaw inVia Confocal Raman Spectrometer, 532 nm laser) were captured from the suspended membranes revealing the D (1345 cm^{-1}) and G (1598 cm^{-1}) peaks (Fig. 1c), which are characteristic of the GO structure [18,27]. X-ray photoelectron spectroscopy (XPS) was also conducted on bulk flakes of the GO (the same flakes that were used to exfoliate the monolayer samples), to analyze the chemical composition and functional structure (Fig. 1d). Fitting to the Lerf–Klinowski model [28], the functional composition of the bulk GO was determined as follows: sp^2 carbon (71.4%), hydroxyl groups (19.3%), carboxyl groups (9.3%). The emission peak for the epoxide group was not detected in meaningful quantities during XPS observation. Since the tested GO membranes appeared void-free, it was further assumed that the carboxyl groups were largely restricted to GO flake edges (XPS spot size was ~400 μm). Under this consideration, the functionalization of GO membranes tested by AFM nanoindentation may be assumed to be purely from hydroxyl groups at a fraction of approximately 20% of available carbon atoms. The carbon-to-oxygen ratio was also calculated from the XPS data to be approximately 4:1. Prior to each nanoindentation measurement of the GO membranes, AFM topographical imaging in tapping mode was performed on the suspended GO membranes using the setup shown schematically in Fig. 2c. The membranes chosen for testing were found to cover the entire hole in the TEM grid, with flake edges clearly visible away from the suspended regions, as shown in Fig. 2a. The monolayer nature of the film was also confirmed by an AFM topography scan at the edge of the GO film. To initiate nanoindentation, the AFM probe was brought into contact at the center of the membrane. Elastic loading and unloading was initially performed in order to collect data for elastic modulus measurements, and also to confirm that slippage did not occur between the membrane and the substrate [8]. The membrane was then indented until failure and was re-imaged in tapping mode after ultimate fracture (Fig. 2b).

Fig. 2d presents the nanoindentation measurements of GO membranes loaded to failure. Breaking loads were measured for seven monolayer GO membranes in the range between 162 and 582 nN with an average breaking load of 324 ± 121 nN. Error is reported in this study as a 95% confidence interval. The tested GO membranes all exhibited similar curvature in their stiffening behavior which highlights the uniformity as well as the homogeneity of the GO membranes. Minor changes in the inflection of loading curves are visible in the region close to fracture of GO membranes. This is likely a result of subcritical cracking within the sample. Examination of post-mortem AFM images shows that the AFM tip had clearly penetrated through the GO membrane.

The elastic properties of the GO membranes were determined following the method reported by Lee et al. [8],

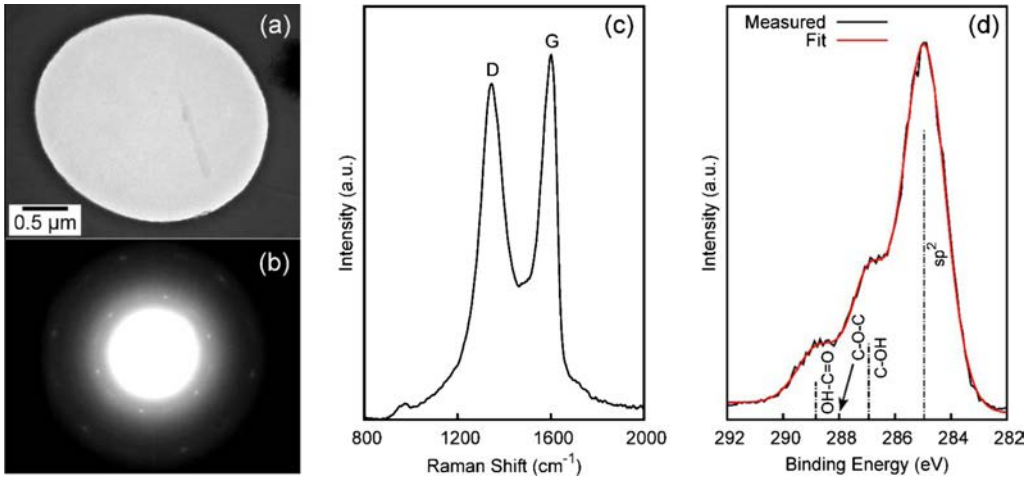

Fig. 1 – (a) Bright field TEM image and (b) SAED pattern of a monolayer GO membrane. The single set of six diffraction spots indicate that a single layer of GO is present. (c) Raman spectrum of a suspended GO membrane. The D (1345 cm^{-1}) and G (1598 cm^{-1}) peaks which are characteristic of GO are clearly visible. (d) XPS spectrum showing the composition of GO functional groups fitted using a Lerf–Klinowski model [28]. The binding energies of the characteristic functional groups are indicated in the figure. The height of each dashed line indicates the relative fractions of each measured functional structure. Excluding the very weak signal from the epoxide groups (C–O–C), the structure of the GO samples is found to be sp^2 carbon (71.4%), hydroxyl (19.3%) and carboxyl (9.3%) groups. (A colour version of this figure can be viewed online.)

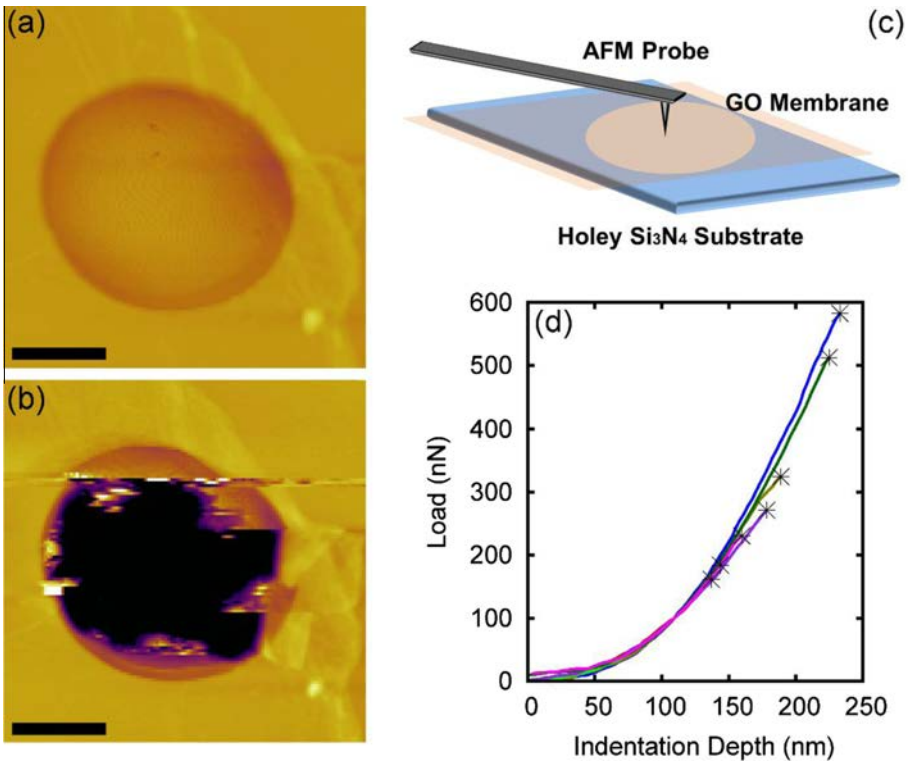

Fig. 2 – AFM images of (a) monolayer GO membrane suspended over a Si_3N_4 TEM grid with 2.5 μm holes and (b) broken monolayer GO membrane after nanoindentation to failure. (c) A schematic of the AFM nanoindentation setup. (d) Load versus indentation depth plots recorded by AFM testing. The markers indicate the breaking load. Scale bar in (a) and (b) is 1 μm. (A colour version of this figure can be viewed online.)

whereby the GO elastic modulus (E) and membrane prestress (σ_o) were calculated analytically through fitting of experimental elastic nanoindentation curves (see Section S3 in the Supplementary data). Fig. S3 presents the elastic response of the tested GO membranes. Although the response is scattered upon initial contact, the GO membranes exhibited similar stiffening behavior, which converges as loading increases. It should be noted that a similar behavior was previously observed for testing of graphene films [8]. Analytical fitting of the collected experimental data yields a 2D elastic modulus of $E^{2D} = 269 \pm 21$ N/m and a membrane prestress of $\sigma_o^{2D} = 91 \pm 10$ mN/m. In 3D terms, estimates of 384 ± 31 GPa and 0.130 ± 0.014 GPa may be calculated for the elastic modulus and prestress of the GO membrane, respectively. A monolayer GO membrane thickness of 0.7 nm [18,29] was used in all 3D stress calculations and referenced GO strengths throughout this paper for the purposes of comparative consistency with existing literature, whereas a thickness of 0.335 nm [8] is assumed in discussions of graphene. This measured 2D elastic modulus is approximately 80% of the value measured for pristine graphene [8] ($E^{2D} = 342$ N/m) and almost twice the stiffness previously reported by Suk et al. [18] for monolayer GO ($E^{2D} = 145.3$ N/m). As the mechanical properties of GO are expected to be highly structurally and chemically dependent, the difference in modulus between the current study and previous reports are likely the result of differences in GO structure and composition [30]. For example, the higher elastic modulus measured in the current study is consistent with a more graphene-like structure due to its lower functionalization (~20% hydroxyl) as compared to the GO membranes studied by Suk et al. (~40%) [18]. In a separate experimental study, Kunz et al. [29] measured GO elastic moduli in the range of 110–420 GPa. Kunz et al. [29] also attributed this large range in stiffness to differences in sample chemistry.

3.2. *Continuum level nanoindentation simulations*

In order to obtain information regarding the in-plane stress state under fracture loading, a continuum-based formulation is required. Following the methodology developed by Lee et al. [9], FE analysis was performed to simulate the AFM nanoindentation process on monolayer GO membranes using the elastic properties obtained from analytical fitting of experimental data. Fig. 3a presents a comparison of the FEM simulation to a representative AFM nanoindentation curve. The close agreement between simulation and experiment permits direct strength assessment by comparing experimental breaking loads with the equibiaxial stress state at equivalent nanoindentation loading in the FE analysis. This continuum-based approach has been previously validated for experimental assessment of strength in polycrystalline graphene [9]. Fig. 3b highlights the relationship between nanoindentation load and in-plane stress. Experimental breaking loads are marked with arrows and were compared with the FEM data in order to extract the experimental strength. From this analysis, the average equibiaxial strength of the tested monolayer GO membranes was found to be 17.3 ± 3.1 N/m

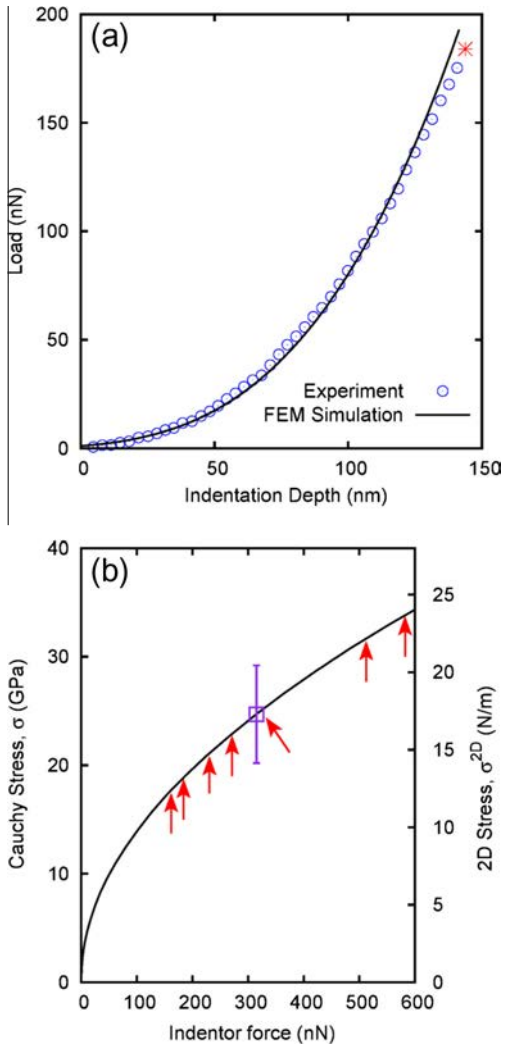

Fig. 3 – (a) Comparison of FEM model to a representative AFM nanoindentation curve, showing good agreement. The breaking load of the monolayer GO membrane is indicated with a star marker. (b) The in-plane equibiaxial stress of indented monolayer GO samples as determined by FEM simulation. Experimental strength was determined by comparing breaking loads to FEM simulation data. The experimental breaking loads are indicated with arrows and the average monolayer GO membrane strength 17.3 ± 3.1 N/m (24.7 ± 4.5 GPa) is indicated with the marker. A 0.7 nm monolayer thickness is assumed in the FEM simulation. (A colour version of this figure can be viewed online.)

(24.7 ± 4.5 GPa). This measured strength is orders of magnitude higher than previously reported strength values for GO papers [22–24] or reduced GO papers [31] and is approximately 50% the reported 2D strength of pristine graphene (34.5 N/m) [9].

3.3. *Theoretical strength of graphene oxide membranes*

Although the strength of monolayer GO has not been previously experimentally measured, first-principles calculations have predicted theoretical strengths reaching well into the GPa range [20,21]. For example, Paci et al. [20] studied a number of GO structures with varied epoxide and hydroxyl functionalizations and predicted theoretical 2D strengths in the range of 14.6–33 N/m (20.9–47.1 GPa) for zigzag-loaded membranes. These numerical predictions are in reasonably good agreement with the experimental findings of the current study. However, as noted in several studies [20,21,29,30], the mechanical properties of GO are chemistry dependent and therefore, structure-specific computational simulations are necessary to determine the theoretical strength of the monolayer GO membranes tested in the current study. Hence, quantum-mechanical simulations using DFT were undertaken to predict the theoretical strength and investigate fracture mechanisms of the monolayer GO samples with the specific functional structure characterized herein.

Using the XPS structural data, a topology was constructed consisting of 20% hydroxyl functionalization and an approximate 4:1 carbon-to-oxygen ratio. The hydroxyl groups were positioned directly above basal plane carbon atoms, following the Lerf–Klinowski model [28]. Carbon sites for hydroxyl bonding were chosen at random, with occupancies above and below the basal plane possessing equal probability for selection. Prior to tensile loading, the GO topology was subjected to variable cell relaxation under a conjugate gradient energy minimization routine in order to achieve a ground state configuration. The relaxed topology of the monolayer GO sample is provided in Fig. 4b. In order to simulate mechanical conditions similar to AFM nanoindentation testing, biaxial tensile simulations were performed with equal strains applied incrementally along the armchair (ac) and zigzag (zz) directions (*i.e.*, $\varepsilon = \varepsilon_{ac} = \varepsilon_{zz}$) [32]. Under this testing protocol, an equibiaxial stress state is measured ($\sigma \approx \sigma_{ac} \approx \sigma_{zz}$), with negligible shear components present in the Cauchy stress tensor (see Supplementary data, Fig. S4). Therefore, the armchair and zigzag tensor components may be considered as the principal stresses, enabling direct comparison to the presented FE analysis. For purposes of comparison, additional uniaxial tensile simulations were performed in the armchair and zigzag directions. This DFT approach has been validated against uniaxial tensile calculations for pristine graphene (see Supplementary data, Fig. S5), and similar supercell sizes have been previously used in DFT studies of defective graphene systems [33]. Failure of GO membranes was identified by elastic instability, which manifested as a large drop in the stress state of the DFT supercell. Previous first-principles calculations have postulated phonon instability as a possible strength-limiting failure mechanism for free-standing graphene membranes [34]. Although this failure pathway cannot be explicitly dismissed, fracture strengths predicted by elastic instability have been shown to agree well with experimental AFM nanoindentation data for suspended graphene membranes [32], supporting the current DFT methodology and analysis. Further investigation may be necessary to identify the dominant mechanisms of mechanical instability in GO under different boundary conditions.

Fig. 4a provides the tensile loading curves of the monolayer GO membrane from DFT calculations. An equibiaxial failure strength of 21.9 N/m (31.3 GPa) is predicted, showing good correlation with the collected experimental data (17.3 ± 3.1 N/m, or 24.7 ± 4.5 GPa in 3D terms). It should be

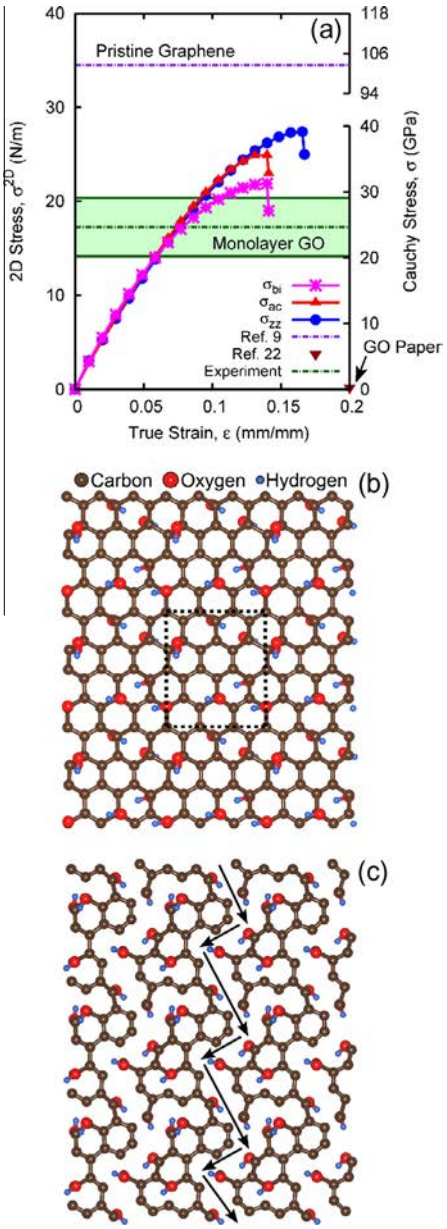

Fig. 4 – (a) Mechanical response of monolayer GO samples as determined by DFT calculations. The equibiaxial strength is calculated to be 21.9 N/m (31.3 GPa) and the uniaxial zigzag and armchair strengths of GO samples are estimated at 24.9 and 27.4 N/m (35.6 and 39.2 GPa), respectively. The average of measured experimental strengths is indicated by the dashed green line and the shaded region represents the 95% confidence interval. The experimental strength of pristine graphene measured by Lee et al. [9] is provided for comparison. The strength of bulk GO papers is also provided in the figure. (b) A schematic of the undeformed GO topology used in DFT calculations. Replica images of the unit cell (dashed line) are shown to highlight the periodic boundary conditions enforced during calculations. (c) Failure morphology (ε = 0.15) of the GO monolayer samples under biaxial loading. Bond cleavage occurs along a path populated by oxygenated carbon atoms as indicated by the arrows. (A colour version of this figure can be viewed online.)

noted that DFT calculations provide a benchmark upper bound for GO mechanical performance as they do not consider any topological defects such as voids which can form during synthesis. This highlights the high quality and near-theoretical strength of the monolayer GO membranes tested here. Fig. 4c illustrates the morphology of bond cleavage post-fracture in the GO membrane after biaxial loading. Bond cleavage occurs along a path populated by functionalized carbon atoms, representing a brittle fracture mechanism. Several transcending cracks are visible in the figure due to the periodicity of the DFT super cell. Under uniaxial testing conditions, theoretical strengths of 24.9 and 27.4 N/m (35.6 and 39.2 GPa) are calculated for armchair and zigzag loaded GO, respectively. In comparison to existing literature, Paci et al. [20] predicted a theoretical zigzag strength of 21.4 N/m (30.6 GPa) for epoxide-hydroxyl functionalized (~70%) monolayer GO with a 2:1 carbon-to-oxygen ratio. Clearly, strength is expected to increase as GO becomes more graphene-like (*i.e.*, higher carbon-to-oxygen ratio), and therefore these results appear consistent with the current study of 4:1 GO membranes. In order to validate the GO topology assumed for computational calculations, the collected DFT tensile data was fit to a polynomial strain energy density function, following the methodology developed in Wei et al. [32] (see Supplementary data, Section S5 and Fig. S5). Fitting of elastic constants to the available DFT data provides an estimate for the sample elastic modulus of E^{2D} = 270 N/m (385.6 GPa), which is in close agreement with the experimentally measured value of 269 N/m (384 GPa). The close agreement between the measured and calculated elastic moduli provides further confidence in the structural assumptions undertaken in DFT simulations and also indicates that the membrane areas tested by nanoindentation likely had a low defect density. It should be noted, however, that the numerous possible topological configurations of the GO supercell is expected to introduce some statistical distribution in theoretical strengths. The results presented here are believed to approximate a weakest-link measurement, as functionalized carbon atoms form a continuous fracture path through the supercell which is available for material failure.

Fig. 4a shows comparisons of the experimental and calculated monolayer GO strengths reported in the current study. The experimentally measured strengths of pristine graphene [9] and GO paper [22] are also highlighted for reference. The current study reports unprecedented strength in monolayer GO membranes, which is orders of magnitude higher than previous measurements for bulk GO paper. The equibiaxial theoretical strength is found to be slightly higher than the experimental results. This result is not surprising since fracture in graphene structures is subject to thermal activation effects [35,36] and therefore, strengths determined under athermal conditions (*i.e.*, DFT simulations) should be larger than experimental measurements at room temperature (300 K). Additionally, the presence of even a small number of defects is known to promote premature failure in 2D systems which may further limit the measureable experimental strength of monolayer GO [37,38]. Most importantly, the current experimental measurement of strength in monolayer GO membranes (17.3 N/m) is approximately 50% the 2D intrinsic strength of pristine graphene (34.5 N/m) [9] which

demonstrates that GO may be utilized as an ultra-strong structural material.

4. Conclusions

The strength of monolayer GO (carbon-to-oxygen ratio of 4:1, ~20% hydroxyl functionalization) was characterized using a combined experimental and theoretical approach. Analytical fitting of AFM nanoindentation tests was employed to determine the elastic properties and prestress of the sampled GO membranes. The results of analytical fitting were used to construct a FEM simulation which informed direct strength measurements of the GO membranes. Through this analysis, the monolayer GO membranes were found to have an average strength of 24.7 GPa, which is orders of magnitude larger than previous reports for GO papers (typically 100s of MPa) and approximately 50% the strength of pristine graphene (when comparing 2D values). Independent DFT calculations were performed to determine the theoretical mechanical properties of the GO membranes. DFT analysis predicted a theoretical equibiaxial strength of 31.3 GPa, with fracture occurring along a path populated by oxygenated carbon atoms. The proximity of experimental measurements and first-principles calculations corroborates the reported strength and indicates that the GO membranes with high carbon-to-oxygen ratios can exhibit near-theoretical strengths.

Acknowledgements

The authors would like to acknowledge funding by the Natural Sciences and Engineering Research Council of Canada (NSERC) through Discovery Grants and the Postgraduate scholarships (PGS) program; and funding from the Canada Foundation for Innovation (CFI). Y.S. also acknowledges financial support from the Canada Research Chairs Program. TEM technical support was provided by Carmen Andrei at the Canadian Center for Electron Microscopy (CCEM). Computations were performed on the Guillimin High Performance Computing (HPC) cluster under the administration of Calcul-quebec and Compute Canada. XPS measurements and analysis were performed with assistance from Hang Chen and Rana Sodhi at Surface Interface Ontario. The authors would like to further thank Professor Glenn Hibbard and the Cellular Hybrid Materials Research Laboratory at the University of Toronto for assistance with ABAQUS simulations.

Appendix A. Supplementary data

Supplementary data associated with this article can be found, in the online version, at http://dx.doi.org/10.1016/j.carbon.2014.09.082.

REFERENCES

[1] Brodie BC. On the atomic weight of graphite. Philos Trans R Soc Lond 1859;149:249–59.
[2] Staudenmaier L. Verfahren zur Darstellung der Graphitsäure. Ber Dtsch Chem Ges 1898;31(2):1481–7.
[3] Hummers WS, Offeman RE. Preparation of graphitic oxide. J Am Chem Soc 1958;80(6):1339.
[4] Hirata M, Gotou T, Horiuchi S, Fujiwara M, Ohba M. Thin-film particles of graphite oxide 1: high-yield synthesis and flexibility of the particles. Carbon 2004;42(14):2929–37.
[5] Park S, Ruoff RS. Chemical methods for the production of graphenes (vol 4, pg 217, 2009). Nat Nanotechnol 2010;5(4):309.
[6] Eda G, Chhowalla M. Chemically derived graphene oxide: towards large-area thin-film electronics and optoelectronics. Adv Mater 2010;22(22):2392–415.
[7] Chen S, Zhu J, Wu X, Han Q, Wang X. Graphene oxide–MnO2 nanocomposites for supercapacitors. ACS Nano 2010;4(5):2822–30.
[8] Lee C, Wei XD, Kysar JW, Hone J. Measurement of the elastic properties and intrinsic strength of monolayer graphene. Science 2008;321(5887):385–8.
[9] Lee G-H, Cooper RC, An SJ, Lee S, van der Zande A, Petrone N, et al. High-strength chemical-vapor-deposited graphene and grain boundaries. Science 2013;340(6136):1073–6.
[10] Zandiatashbar A, Lee GH, An SJ, Lee S, Mathew N, Terrones M, et al. Effect of defects on the intrinsic strength and stiffness of graphene. Nat. Commun. 2014:5.
[11] Tapia A, Peón-Escalante R, Villanueva C, Avilés F. Influence of vacancies on the elastic properties of a graphene sheet. Comput Mater Sci 2012;55:255–62.
[12] Wang MC, Yan C, Ma L, Hu N, Chen MW. Effect of defects on fracture strength of graphene sheets. Comput Mater Sci 2012;54:236–9.
[13] Riccardo Dettori, Emiliano Cadelano, Luciano C. Elastic fields and moduli in defected graphene. J Phys: Condens Matter 2012;24(10):104020.
[14] Xiao JR, Staniszewski J, Gillespie Jr JW. Tensile behaviors of graphene sheets and carbon nanotubes with multiple Stone–Wales defects. Mater Sci Eng, A 2010;527(3):715–23.
[15] Zhang L, Wang Z, Xu C, Li Y, Gao J, Wang W, et al. High strength graphene oxide/polyvinyl alcohol composite hydrogels. J Mater Chem 2011;21(28):10399–406.
[16] Ding Q, Liu B, Zhang Q, He Q, Hu B, Shen J. Synthesis and characterization of polyurethane/montmorillonite nanocomposites by in situ polymerization. Polym Int 2006;55(5):500–4.
[17] Gomez-Navarro C, Burghard M, Kern K. Elastic properties of chemically derived single graphene sheets. Nano Lett 2008;8(7):2045–9.
[18] Suk JW, Piner RD, An J, Ruoff RS. Mechanical properties of monolayer graphene oxide. ACS Nano 2010;4(11):6557–64.
[19] Cao C, Sun Y, Filleter T. Characterizing mechanical behavior of atomically thin films: a review. J Mater Res 2014;29(03):338–47.
[20] Paci JT, Belytschko T, Schatz GC. Computational studies of the structure, behavior upon heating and mechanical properties of graphite oxide. J Phys Chem C 2007;111(49):18099–111.
[21] Liu L, Zhang J, Zhao J, Liu F. Mechanical properties of graphene oxides. Nanoscale 2012;4(19):5910–6.
[22] Dikin DA, Stankovich S, Zimney EJ, Piner RD, Dommett GHB, Evmenenko G, et al. Preparation and characterization of graphene oxide paper. Nature 2007;448(7152):457–60.
[23] Wang C, Frogley MD, Cinque G, Liu L-Q, Barber AH. Deformation and failure mechanisms in graphene oxide paper using in situ nanomechanical tensile testing. Carbon 2013;63:471–7.
[24] Park S, Lee K-S, Bozoklu G, Cai W, Nguyen ST, Ruoff RS. Graphene oxide papers modified by divalent ions—enhancing mechanical properties via chemical cross-linking. ACS Nano 2008;2(3):572–8.

[25] Giannozzi P, Baroni S, Bonini N, Calandra M, Car R, Cavazzoni C, et al. QUANTUM ESPRESSO: a modular and open-source software project for quantum simulations of materials. J Phys: Condens Matter 2009;21(39):395502.
[26] Perdew JP, Burke K, Ernzerhof M. Generalized gradient approximation made simple. Phys Rev Lett 1996;77(18):3865–8.
[27] Kudin KN, Ozbas B, Schniepp HC, Prud'homme RK, Aksay IA, Car R. Raman spectra of graphite oxide and functionalized graphene sheets. Nano Lett 2007;8(1):36–41.
[28] He H, Klinowski J, Forster M, Lerf A. A new structural model for graphite oxide. Chem Phys Lett 1998;287(1–2):53–6.
[29] Kunz DA, Feicht P, Godrich S, Thurn H, Papastavrou G, Fery A, et al. Space-resolved in-plane moduli of graphene oxide and chemically derived graphene applying a simple wrinkling procedure. Adv Mater 2013;25(9):1337–41.
[30] Gomez-Navarro C, Meyer JC, Sundaram RS, Chuvilin A, Kurasch S, Burghard M, et al. Atomic structure of reduced graphene oxide. Nano Lett 2010;10(4):1144–8.
[31] Zhu J, Zhang H, Kotov NA. Thermodynamic and structural insights into nanocomposites engineering by comparing two materials assembly techniques for graphene. ACS Nano 2013;7(6):4818–29.
[32] Wei X, Kysar JW. Experimental validation of multiscale modeling of indentation of suspended circular graphene membranes. Int J Solids Struct 2012;49(22):3201–9.
[33] Yadav S, Zhu Z, Singh CV. Defect engineering of graphene for effective hydrogen storage. Int J Hydrogen Energy 2014;39(10):4981–95.
[34] Marianetti CA, Yevick HG. Failure mechanisms of graphene under tension. Phys Rev Lett 2010;105(24):245502.
[35] Zhao H, Aluru NR. Temperature and strain-rate dependent fracture strength of graphene. J Appl Phys 2010;108(6).
[36] Daly M, Singh CV. A kinematic study of energy barriers for crack formation in graphene tilt boundaries. J Appl Phys 2014;115(22).
[37] Wei X, Fragneaud B, Marianetti CA, Kysar JW. Nonlinear elastic behavior of graphene: Ab initio calculations to continuum description. Phys Rev B 2009;80(20):205407.
[38] Grantab R, Shenoy VB, Ruoff RS. Anomalous strength characteristics of tilt grain boundaries in graphene. Science 2010;330(6006):946–8.